Journal of Nondestructive Evaluation (2024) 43:95
https://doi.org/10.1007/s10921-024-01111-7

Classification of Practical Floor Moisture Damage Using GPR - Limits and Opportunities

Tim Klewe[1] · Christoph Strangfeld[1] · Tobias Ritzer[2] · Sabine Kruschwitz[1,3]

Received: 1 March 2024 / Accepted: 23 July 2024 / Published online: 10 August 2024

Abstract
Machine learning in non-destructive testing (NDT) offers significant potential for efficient daily data analysis and uncovering previously unknown relationships in persistent problems. However, its successful application heavily depends on the availability of a diverse and well-labeled training dataset, which is often lacking, raising questions about the transferability of trained algorithms to new datasets. To examine this issue closely, the authors applied classifiers trained with laboratory Ground Penetrating Radar (GPR) data to categorize on-site moisture damage in layered building floors. The investigations were conducted at five different locations in Germany. For reference, cores were taken at each measurement point and labeled as (i) dry, (ii) with insulation damage, or (iii) with screed damage. Compared to the accuracies of 84 % to 90 % within the laboratory training data (504 B-Scans), the classifiers achieved a lower overall accuracy of 53 % for on-site data (72 B-Scans). This discrepancy is mainly attributable to a significantly higher dynamic of all signal features extracted from on-site measurements compared to laboratory training data. Nevertheless, this study highlights the promising sensitivity of GPR for identifying individual damage cases. In particular the results showing insulation damage, which cannot be detected by any other non-destructive method, revealed characteristic patterns. The accurate interpretation of such results still depends on trained personnel, whereby fully automated approaches would require a larger and diverse on-site data set. Until then, the findings of this work contribute to a more reliable analysis of moisture damage in building floors using GPR and offer practical insights into applying machine learning to non-destructive testing for civil engineering (NDT-CE).

Keywords GPR · Material moisture · Building floor · Classification · Machine learning

1 Introduction

Non-destructive testing in civil engineering (NDT-CE) often involves examining large areas, including various local incidents of damage. These examinations produce a significant amount of data that require thorough analysis by experienced personnel. Applying machine learning methods could help to not only speed up these processes, but may also provide deeper insights into the data structure and uncover yet unknown relationships within NDT-CE. However, the effective use of these emerging techniques depends on a rich and diverse training data set. In contrast to successful examples in computer vision applications like autonomous driving or facial recognition, the availability of labeled non-destructive testing (NDT) data is often limited, which poses the risk of an inadequate representation of the space of possibilities [1]. Unfortunately, referencing training data for machine learning is not always straight forward for NDT-CE. To address these challenges, this work creates referenced training data within laboratory conditions to classify new, also referenced on-site measurements. The results of this validation aim to give practical insight into the application of machine learning in NDT-CE. Thereby, the study focuses on moisture damage in layered building floors, which present a research topic of relevant interest.

From 2003 to 2022, the yearly costs of pipe water damage in Germany increased by 163 % to a total of 3.8 billion Euros [2]. Often, the actual extent of a moisture damage is not fully recognized, leading to costly deterioration of building struc-

✉ Tim Klewe
tim.klewe@bam.de

[1] Bundesanstalt für Materialforschung und -prüfung, Unter den Eichen 87, 12205 Berlin, Germany

[2] Ingenieurbüro Tobias Ritzer GmbH, Lindenbachstraße 29, 91126 Schwabach, Germany

[3] Technische Universität Berlin, Gustav-Meyer-Allee 25, 13355 Berlin, Germany

tures. The additional risk of mold also threatens the health of residents [3, 4], which highlights the need for a quick and accurate diagnosis of damage.

For pipe water damage, building floors are the most affected structure, as they either contain the broken pipe system within their insulation or get flooded from above. This leads to two primary types of damage: wet insulation or wet screed. Moisture barriers, usually made of polyethylene foils, generally prevent water from moving between these layers. However, in the rare case of a poor functionality, also both layers may be damaged at the same time. Generally, knowing the presence and distribution of these different types of damage is crucial for performing efficient and effective repairs.

Most common non-destructive moisture measurement methods [5, 6], like resistivity-based, capacitive, or thermal methods, are not adequate for an in-depth examination of building floors. They typically yield moisture information only for surface areas and may be hindered by the layer structure of the floor. Furthermore, floor structures often include a layer on top of screed and insulation (carpet, laminate, etc.), which can disturb the accuracy of the applied method. In particular, the moisture condition of the insulation, which is the deeper layer, is not detected by most methods and presents a special challenge in moisture investigations on building floors.

A suitable exception is the Neutron probe [7], as it can reach penetration depths of almost 30 cm. However, it only gives integral measurements of the investigated area and cannot provide detailed information about different depths. Further, it is not possible to distinguish between chemically bound and liquid water, making it necessary to extract cores, which is time-consuming and costly, to calibrate the data.

So far, Ground Penetrating Radar (GPR) is the most promising non-destructive method to provide the important depth information necessary to classify moisture damage in building floors. Commonly used in geophysics [8, 9], it is increasingly applied in civil engineering (CE) [10, 11], also for moisture measurements on building materials like asphalt [12, 13], concrete [14–17], bricks [18, 19], and screed [20]. A short overview about the principle of moisture measurements with GPR is given in the following section.

1.1 Moisture Measurement with GPR

By transmitting and receiving electromagnetic (EM) waves, GPR represents a suitable and sensitive method for material moisture measurement. The key factor in this process is the material's relative permittivity ε_r [21, 22], which is greatly affected by the amount of water present within an investigated area. This is due to the significant difference in ε_r between dry building materials like concrete, which ranges from 4 to 10 [23], and water, which has a value around 81 [24]. As a result, higher moisture levels lead to increased relative permittivities in a medium, with wet concrete showing values between 10 and 20. These changes greatly influence the propagation characteristics of EM waves, leading to noticeable lower amplitudes, longer travel times and lower frequencies of the signal received. By analyzing these signal characteristics, it is possible to make informed estimates about the moisture content in the material. A specific review is given in [25], providing further literature about various applications of GPR for moisture measurements in CE.

1.2 Preceding Laboratory Study

In a previous study by Klewe et al. [26], a laboratory investigation was carried out to examine common damage cases in floor constructions using GPR. Here, a modular specimen, shown in Fig. 1, was used to enable an interchangeable test setup. With that, the diverse practice of real floor construction was modeled by varying the layer thicknesses and materials of the screed and insulation layer, as listed in Table 1.

The experiment simulated three scenarios for classification: (i) dry, (ii) insulation damage, and (iii) screed damage. The variety of materials and thicknesses (Table 1) allows for the simulation of 84 different floor constructions for each of the three scenarios. This resulted in a data set of 252 measurements or 504 B-scans (with each measurement consisting of two orthogonal survey lines). This data set was then used to develop a strategy for identifying different types of damage. It involved the extraction of significant features to train various classifiers, which are also employed in this study and will be briefly discussed later in Sect. 2.2.

The previous study achieved high classification accuracies, ranging from 84 % to 88 %. This demonstrated the potential and sensitivity of GPR to identify different moisture damage scenarios in building floors. However, the direct applicability of these methods and findings to real damage cases in actual floor constructions remains an open question. Addressing this question is the primary focus of the following on-site study.

2 Methods

2.1 On-Site Measurements

The on-site investigations of real floor damages were carried out at five different locations in Germany. The sites included a recreation center, a restaurant, a community center, a student residence, and a parking garage. As matter of clarity, the measurements from these locations are referred to by their respective cities: (i) Berlin, (ii) Grossenseebach, (iii) Nürnberg, (iv) Pegnitz, and (v) Wunsiedel.

A consistent procedure was implemented across all the locations: a grid of numbered measurement points (MPs) was

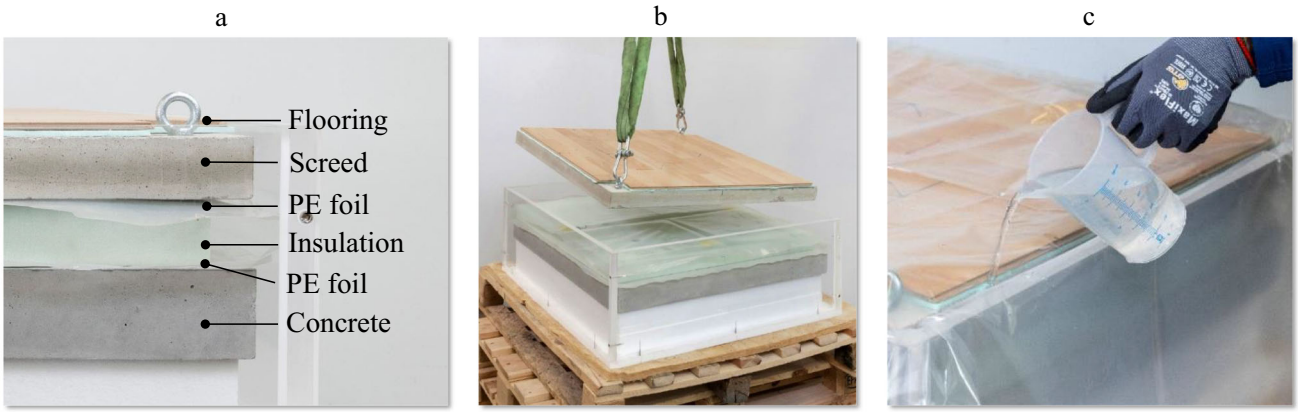

Fig. 1 Modular test specimen with screed, insulation, and concrete base layer (**a**, **b**) and the simulation of an insulation damage by adding water to the setup (**c**) [27]

Table 1 Used materials and layer thicknesses for the screed (top) and insulation layer (bottom) [26]

Material	Thickness D [cm]
Cement screed (CT)	5, 6, 7
Anhydrite screed (CA)	5, 6, 7
Expanded polystyrene (EP)	2, 5, 7, 10
Extruded polystyrene (XP)	2, 5, 7, 10
Glass wool (GW)	2, 6, 10
Perlites (PS)	2, 6, 10

marked in each room under investigation. Depending on the room layout and access, MPs spacing ranged from approximately 1.5 m to 3 m. As shown in Fig. 2 a, each MP was located at the crossing point of two orthogonal GPR survey lines (B-scans), 50 cm long each. GPR data were collected using a 2 GHz antenna and GSSI SIR 20 GPR system set with a spatial sampling of 250 A-scans per meter (A-scans spacing of 4 mm) and to record over a time window of 11 ns (512 temporal samples).

After conducting the GPR measurement, a core of 6.8 cm diameter was extracted at each MP, reaching from the floor surface to the bottom of the insulation layer, as shown in Fig. 2 b. Screed and insulation materials were immediately separated and stored in two plastic bags to prevent water evaporation. Later, their moisture content was determined by oven drying and weighing, following the Darr method [28]. The obtained values in wt% then provide a reference for the GPR surveys. Here, moisture values exceeding 4 % in cement screed and 15 % in insulation indicated damage to these specific layers. This reference information was then used to label each survey line (or B-scan) according to the actual damage detected. If damages were found in both layers, which was not included in the laboratory study, the measurement was labeled as screed damage. This labeling was based on the premise that the screed, being the top layer, would primarily affect the emitted EM waves.

2.2 Feature Extraction

This work aims to validate a laboratory method by applying it on real damage cases. Therefore, the same features identified in Klewe et al. [26] are used. A comprehensive overview of the different features commonly used in GPR moisture measurements is also given in [25]. The following section gives a brief presentation of the strategy used within this study:

GPR measurements on building floors typically reveal three distinct wave phases, each originating from specific areas within the structure. This is demonstrated by an typical A-scan in Fig. 3 b. The direct wave (DW) travels the shortest path from transmitter to receiver and is therefore measured first. Partly traveling over air and the surface, it is sensitive to superficial screed moisture. The first reflected wave (RW1) emerges from the screed-insulation interface, while the second reflected wave (RW2) originates from the insulation-concrete interface. RW1 is sensitive to both screed and insulation damages, whereas RW2 is more influenced by insulation moisture. The laboratory study summarized in Sect. 1.2 identified the following five A-scan features used to classify moisture damage in building floors:

- Feature F_1: A_{DW} - Amplitude of the direct wave [13–15]
- Feature F_2: A_{RW2} - Amplitude of the 2^{nd} reflection [13–15]
- Feature F_3: f_{RW2} - Dominant frequency of the 2^{nd} reflection [18, 29]
  (Short-time Fourier transform: hamming: hamming window size=1.29 ns; overlap=1.27 ns)
- Feature F_4: A_{RW1}/A_{DW} - Ratio of the amplitudes of the 1^{st} reflection and direct wave [16]

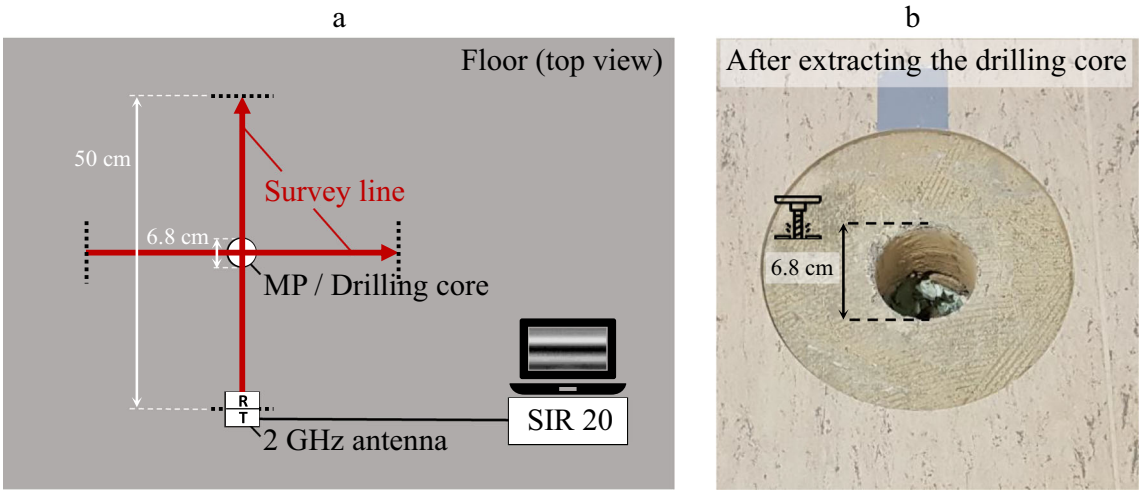

Fig. 2 GPR survey lines (**a**) around a measurement point from which the reference core is extracted (**b**). Two 50 cm radar survey lines are collected with the SIR 20 from GSSI and a 2 GHz antenna [27]

- Feature F_5: f_{RW1}/f_{DW} - Ratio of the dominant frequencies of the 1^{st} reflection and direct wave

These features are influenced not only by moisture but also by variables like layer thicknesses of screed and insulation, and their respective materials. In on-site investigations, these parameters are often unknown, making decisions based on mere thresholds for these features impractical. Thus, the variation of A-scan features within a single survey line (or B-scan) is further analyzed, as depicted in Fig. 3. It was observed in the laboratory that dry floor constructions exhibit no deviations for a specific feature across an entire B-scan. However, the presence of water affects the reflected waves, causing variations as shown by an example of insulation damage in Fig. 3 c. Statistical measures like standard deviation and range were employed to convert the vectorial A-scan features into scalar B-scan features (Fig. 3 d, effectively distinguishing damage cases within the laboratory data set. This was achieved by training different classifiers, which shall now be tested on the collected on-site data.

2.3 Classification

To evaluate the method transferability to practical scenarios, this study utilizes classifiers trained with laboratory data from the previous research mentioned in Sect. 1.2. The Python scikit-learn library [30] is used to implement a multinomial logistic regression (MLR), a random forest (RF), a support vector machine (SVM), and an artificial neural network (ANN), all in their standard configurations (default parameters only). Trials conducted during the previous study showed that the selection of appropriate signal features had a much greater impact on classifier performance than the adjustment of specific model parameters. In addition, since all models consistently achieved similar accuracy values in the laboratory study, there was no indication that selecting different models or model parameters would yield significantly better results.

Compared to the laboratory study, the training process was slightly adjusted for the application on on-site data. Rather than randomly splitting the data into training and test samples, groups of likely dependent measurements are defined to serve as separate test data. Therefore, a specific material (screed or insulation) with a certain thickness characterizes each group. For example, all measurements with a 5 cm EP insulation or a 7 cm CA screed are excluded from the training data and utilized as test data. Given the variations in Table 1, this results to a total of 20 groups. In the laboratory study, almost all of the setups with 2 cm insulation in the floor construction contained no water in the measured area, as the small amount of added water was trapped in the unmeasured outer edges of the specimen. Elimination of these unrepresentative measurements resulted in an improvement in accuracy, so these cases are also removed here. Consequently, subsets of 16 groups are used to train and test each of the four classifiers, leading to 64 trained models. Before training, data standardization is conducted using the *StandardScaler* from scikit-learn for mean removal and achieving unit variance. This standardization is crucial to prevent any feature with higher magnitude from exerting unreasonable influence.

The achieved mean accuracies of 84 % to 90 % by the classifiers were comparable to those from the preceding study, which suggests a sufficient independence of test and training data when performing random splits. The challenge of applying trained classifiers to entirely new data comes from their limited ability to extrapolate beyond the scope of the training data. The effectiveness of these classifiers depends

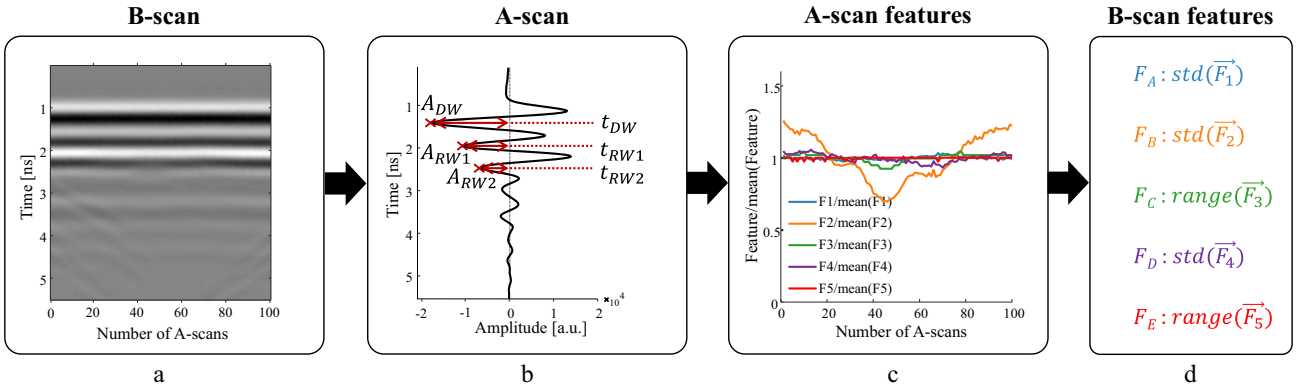

Fig. 3 Procedure for extracting A- and B-scan features as described in [26] and [27]

on how well the training samples represent the full space of possibilities. Since the training data set is derived from an experimental program, it may not cover a sufficient range within this space, leading to significant variance in predictions for new, potentially more distant data points. To address this problem, all 64 classifiers are used to evaluate the newly obtained on-site measurement data. Here, each classifier type (MLR, RF, SVM, and ANN) constitutes a 'voting group' of 16 models. The final classification is determined by the voting group that shows the highest consistency, defined as the group with the highest number of identical predictions. This approach, known as bootstrap aggregating (or bagging) [31], is employed to ensure more stable and accurate classifications of unknown on-site data. As the laboratory data, the on-site data undergoes standardization using the same *StandardScaler* that was fitted and used for the laboratory training data.

3 Results

A total of 186 MPs (372 B-Scans) were collected from the five on-site locations across Germany. The distribution of these points was as follows: Berlin with 29 MPs, Grossenseebach with 33 MPs, Nürnberg with 44 MPs, Pegnitz with 48 MPs, and Wunsiedel with 32 MPs. Based on the analysis of the extracted cores, the MPs were categorized, with 50 labeled as dry, 45 as having insulation damage, and 93 as showing screed damage. This section will first provide an overview of the general characteristics observed in the measured data, followed by a detailed analysis of the achieved classification results.

3.1 On-Site Measurements

Figs. 4, 5, and 6 present representative on-site measurements of building floors, each corresponding to one of the three damage scenarios: dry, insulation damage, and screed damage, respectively. Within each figure, two collected B-scans are displayed, alongside their extracted A-scan features. For each MP where a core was extracted, the layer thicknesses and moisture contents for both screed and insulation are noted in the bottom right corner of each B-scan. Core positions are indicated on each B-scan by light gray vertical bars.

Example a) in Fig. 4 shows a measurement labeled as dry, similar to those collected in the laboratory study (also depicted later in Fig. 11). The B-scan in this case exhibits minimal horizontal deviations for DW, RW1 and RW2, suggesting absence of water or seemingly uniform conditions in the area under investigation. However, the extracted A-scan features reveal variations in F_2, F_4, and F_5, which include all wave phases discussed in Sect. 2.2. This is in contrast to the smoother and flatter patterns seen in the laboratory data, hinting at a potentially higher heterogeneity in the on-site material parameters, such as layer thickness or moisture content. This hypothesis is further supported by the second dry example in Fig. 4 b. Here, the B-scan displays more pronounced horizontal variations, which are also reflected in the A-scan features. Notably, the increase in travel time in the latter half of the survey line could be attributed to either an increase in screed thickness or a rise in screed moisture content. However, the concurrent decrease in the amplitude of DW (indicated by the blue F_1) suggests an increase in moisture content rather than a change in thickness. This is because DW is particularly sensitive to superficial screed moisture and is not affected by the underlying layer thickness.

The core extracted from MP 31 in Nürnberg, as shown in Fig. 5 a, successfully identified a damaged insulation with a moisture content of 120 wt%. The corresponding GPR measurement for this MP also shows notable amplitude fluctuations for RW1 and RW2, while DW remains relatively constant. Such attenuation patterns in RW1 and RW2 are typical for water presence in the insulation layer, which could also be observed in the laboratory study. In contrast, the GPR data from MP 36, while showing similar effects, are not as pronounced as in MP 31. In addition to RW1 and

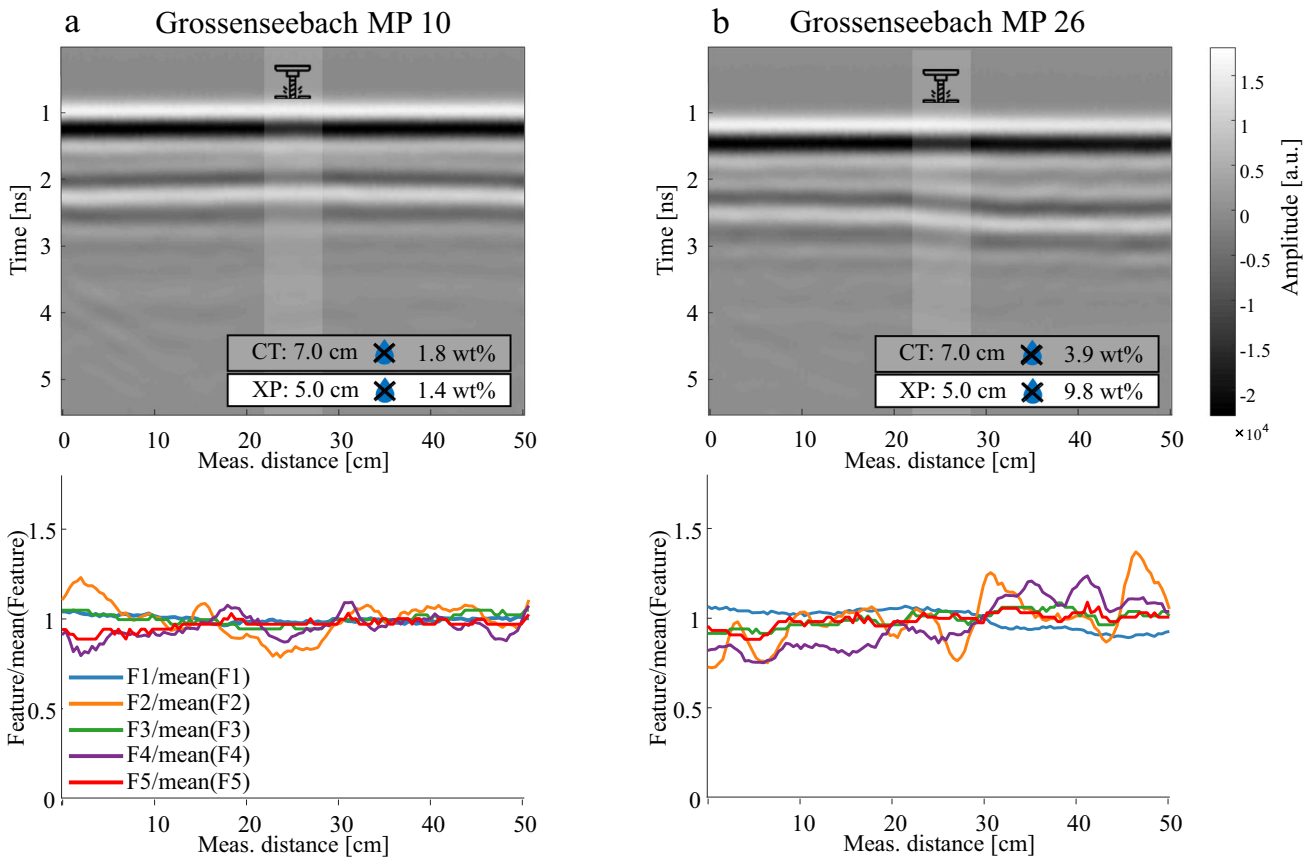

Fig. 4 Example B-scans (top) and their respective A-scan feature charts (bottom) collected on dry floors in Grossenseebeach. The light gray vertical bar in the centre of the B-scans marks the location of the extracted core. Thickness and moisture content of screed and insulation layers are reported at the bottom right of the B-scans [27]

RW2, slight deviations are observed in DW. This variability complicates the interpretation of the radar data, which could be misinterpreted as either a dry condition or screed damage. Nevertheless, the increased dynamics in features F_2 and F_4 from 20 cm to 50 cm, while F_1 remains relatively unchanged, suggest the likelihood of insulation damage.

Figure 6 shows two characteristic measurements from floors with screed damage, each displaying relatively high moisture contents of 7 wt%. A key indication in both cases is the significantly attenuated DW, evident from the reduced contrast between 1 ns and 2 ns in both B-scans. However, this threshold-based amplitude feature is not directly captured by the applied feature extraction strategy, which focuses on statistical measures across the horizontal axis. The difference in attenuation becomes apparent only when these measurements are compared with dry reference MPs, like those in Fig. 4. Without such comparisons, the observed patterns could potentially be attributed to other factors, such as a more attenuating floor cover or a lower gain setting in the GPR system. Nonetheless, the integral measuring principle of GPR reflections allows screed damage to impact all wave phases under consideration. Consequently, variations in every feature, as observed in both examples in Fig. 6, are indicative of screed damage.

In addition to the inherent uncertainties in on-site moisture measurements with GPR, several challenges were encountered during the investigations. A common issue was the presence of floor heating systems, as illustrated in Fig. 7. Located directly beneath the screed, these systems disrupt the expected reflection of RW1, making it difficult to apply the established analysis strategy. As a result, any measurements with clear signs of existing floor heating were excluded from the dataset. Unfortunately, this was the case for nearly all the measurement points in Pegnitz, Wunsiedel, and Berlin, leading to the exclusion of these data sets from subsequent classification model applications. However, it is worth noting that in instances like those observed in Wunsiedel, the visibly increased attenuation associated with higher moisture levels could still provide insight into screed damage. However, this aspect was not further investigated within the scope of this work.

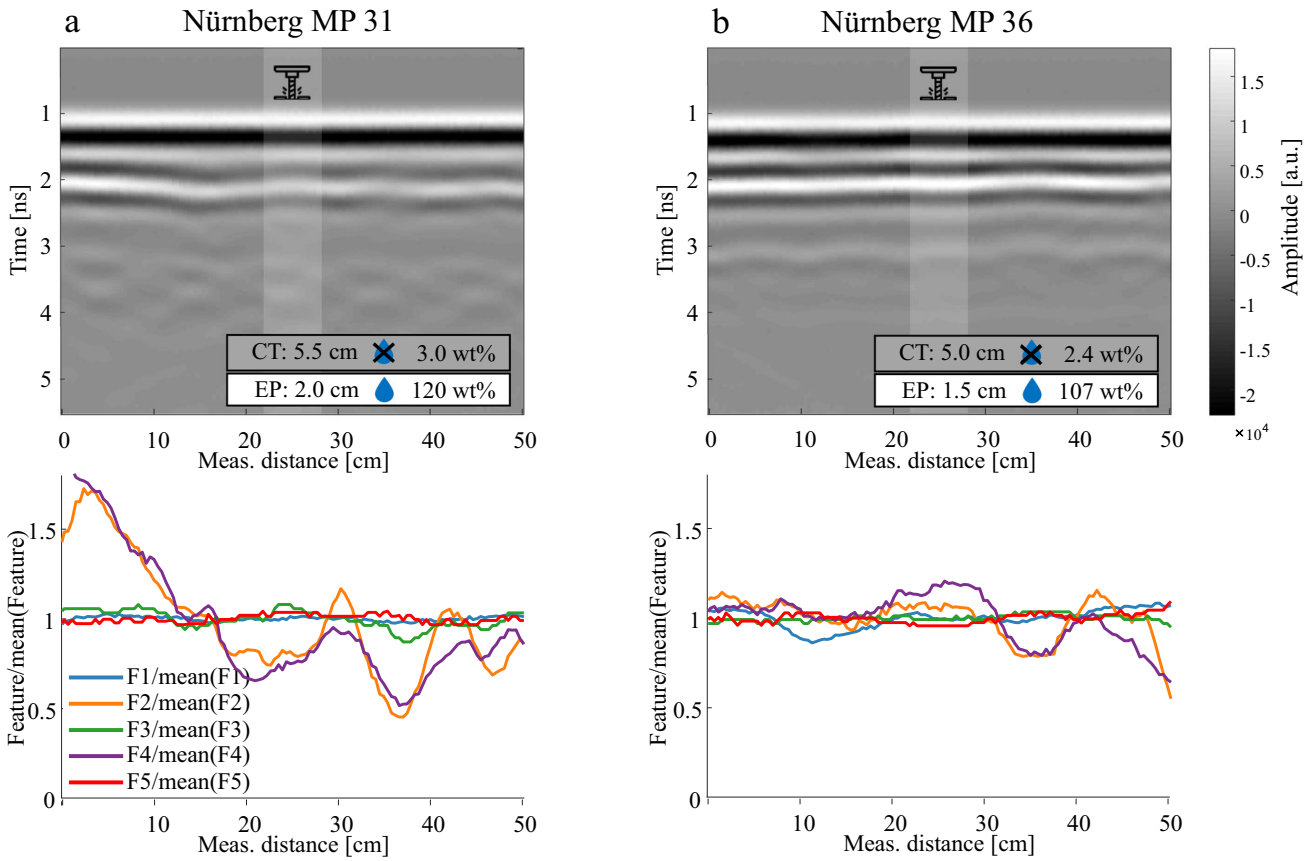

Fig. 5 Example B-scans (top) and their respective A-scan feature charts (bottom) collected on floors with insulation damage in Nürnberg. The light gray vertical bar in the centre of the B-scans marks the location of the extracted core. Thickness and moisture content of screed and insulation layers are reported at the bottom right of the B-scans [27]

Within the Grossenseebach measurements, an additional complication arose from a screed reinforcement mesh in eight MPs, which can be seen in Fig. 8. The hyperbolic reflection patterns originating from this mesh resemble floor heating but show much closer spacing. Due to the interference caused by these metallic elements, all affected measurements were excluded from the Grossenseebach dataset. In Nürnberg, the presence of a steel beam crossing the survey line significantly impacted the B-scans of seven MPs, as shown in Fig. 9. Additionally, this beam was situated in a room lacking insulation in the floor structure. Given that such a scenario was not included in the laboratory study, the twelve MPs gathered in this area were also excluded from the analysis.

3.2 Classification of On-Site Measurements

The analysis focused solely on on-site measurements from Grossenseebach and Nürnberg, after excluding data affected by screed reinforcement, steel beams, and absent insulation layers. The refined data sets included 50 and 62 B-scans from 25 and 31 MPs in Grossenseebach and Nürnberg, respectively. Feature extraction, as detailed in Sect. 2.2, was then applied to these datasets. However, it was not always possible to detect all five features in each measurement. In some B-scans, highly attenuated or interfered wave phases hindered clear separation or identification, leading to NaN-values for the affected features. Consequently, additional 24 B-Scans from Grossenseebach and 16 from Nürnberg were discarded, leaving 26 and 46 B-scans available for analysis.

This reduction in usable data highlights significant limitations in automated classification of on-site GPR measurements. Despite these challenges, the remaining measurements underwent classification based on their extracted features. Figure 10 shows the achieved accuracies and confusion matrices for both data sets. The overall accuracies of 46.2 % for Grossenseebach and 56.5 % for Nürnberg are significantly below those achieved on the laboratory data, laying between 84 % and 90 %. Such a difference often indicates a problem with overfitting the training data [32]. The confusion matrices reveal that most measurements in both data sets

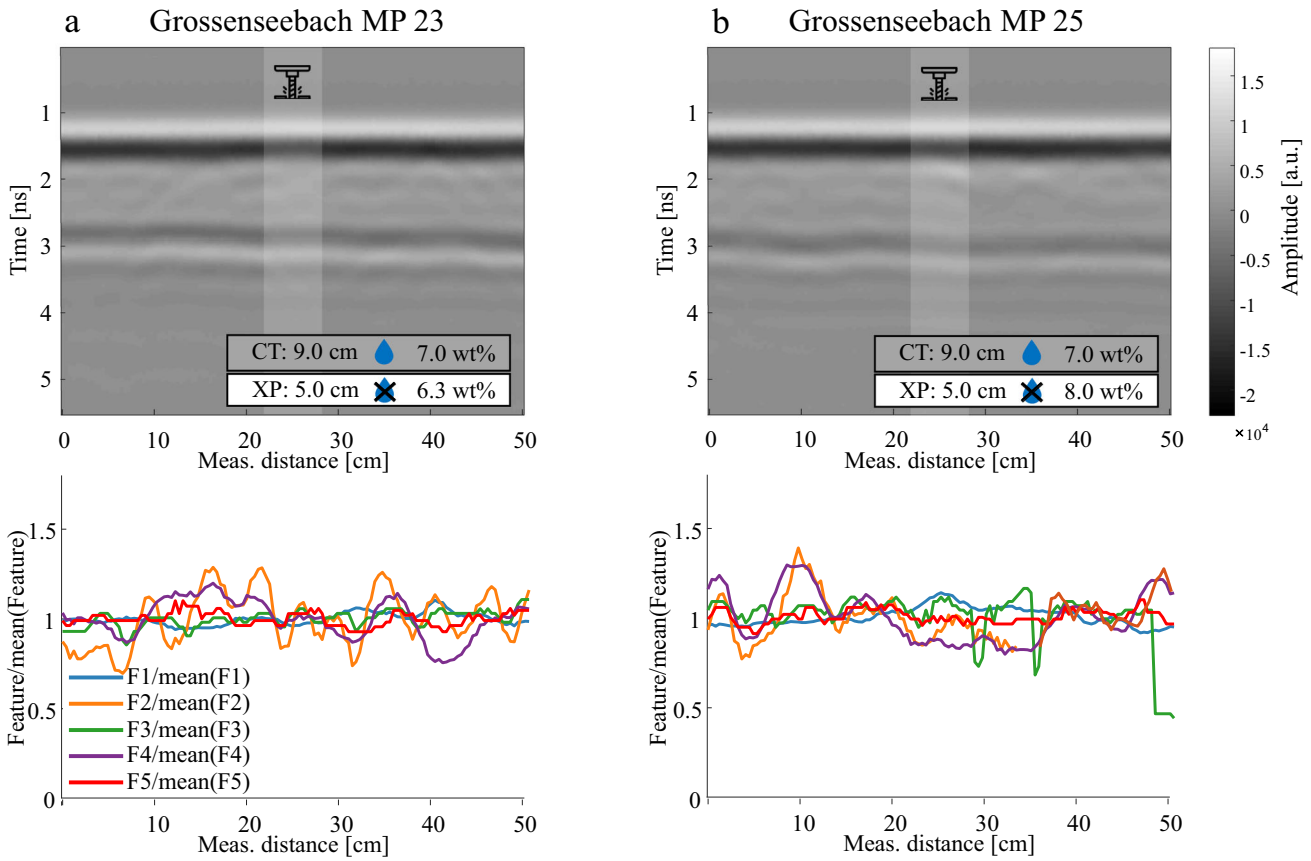

Fig. 6 Example B-scans (top) and their respective A-scan feature charts (bottom) collected on floors with screed damage in Grossenseebach. The light gray vertical bar in the centre of the B-scans marks the location of the extracted core. Thickness and moisture content of screed and insulation layers are reported at the bottom right of the B-scans [27]

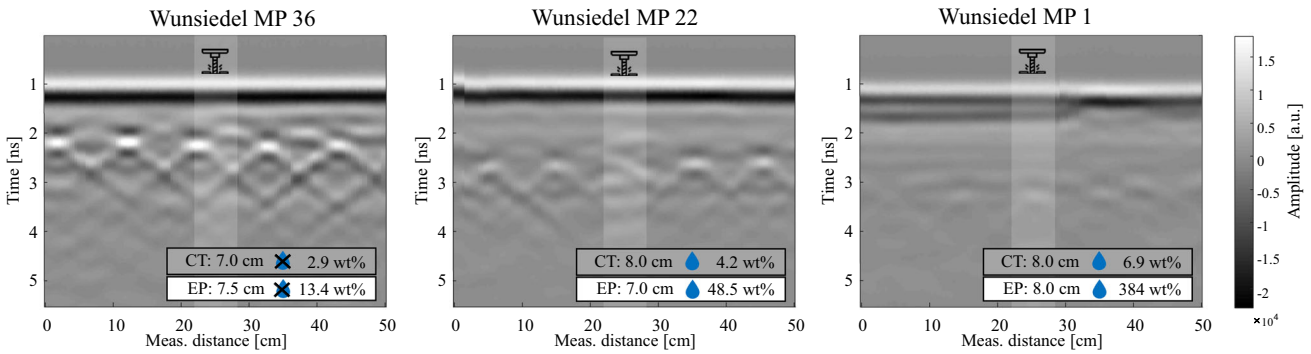

Fig. 7 Sample B-scans showing underfloor heating systems in Wunsiedel. The moisture contents for both, screed and insulation, rise from left to right [27]

were predominantly classified as screed damage. This trend raises questions about the actual sensitivity and effectiveness of the classification process. It remains unclear whether the classification accurately reflects a high sensitivity for detecting screed damage, or if the observed higher hit rate is merely coincidental, influenced by the prevalence of screed damage cases in the data sets.

When applied to new on-site data, the automatic classification trained with laboratory data fell short of replicating laboratory-level accuracy. The reasons behind this perfor-

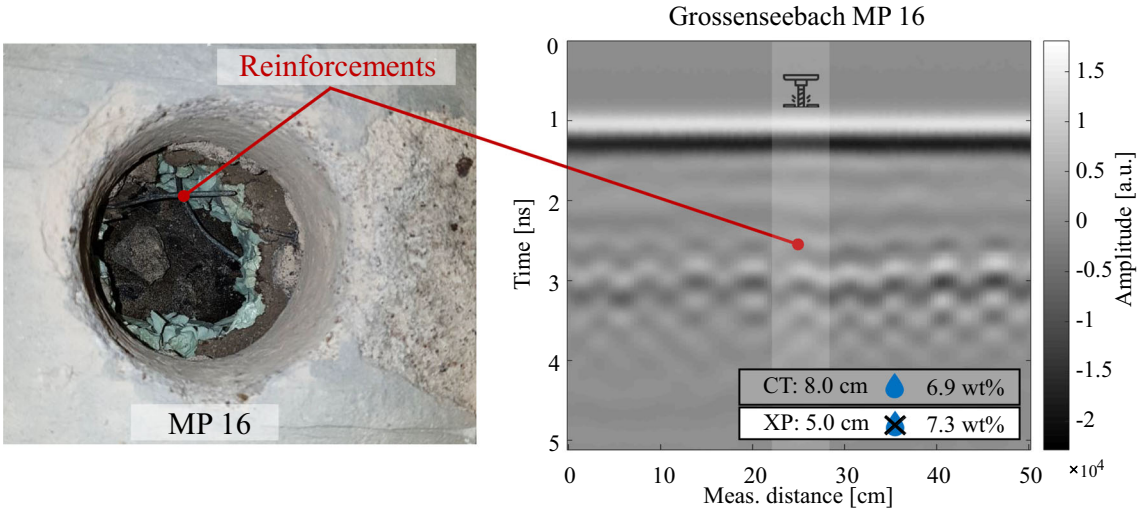

Fig. 8 Screed reinforcement mesh visible inside the drilling hole of MP 16 (left) and in the respective B-scan (right) [27]

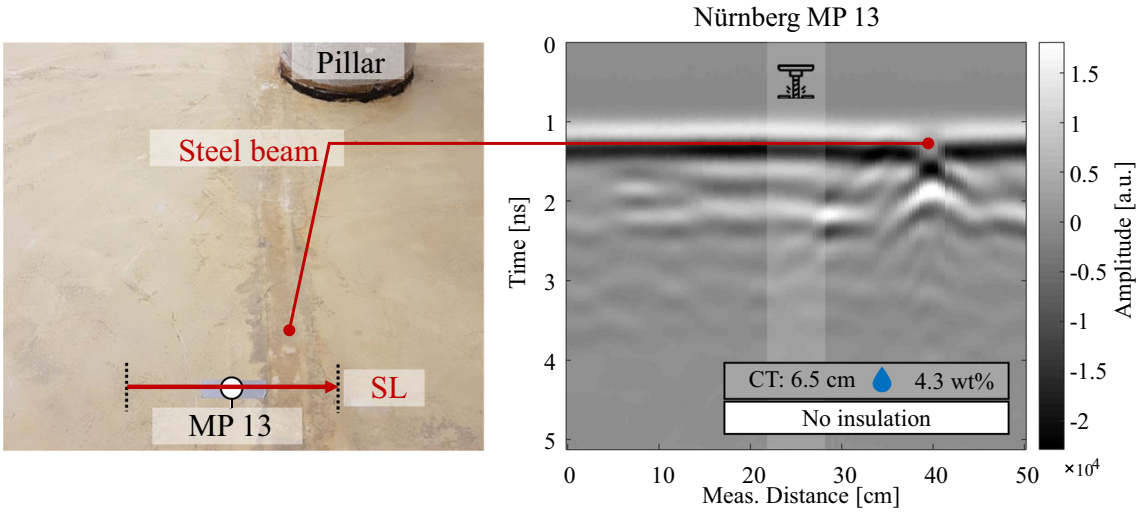

Fig. 9 Steel beam crossing the MP 13 survey line (SL) in Nürnberg (left) and the respective B-scan (right) [27]

mance gap will be explored in the subsequent section through an in-depth analysis of the data sets. This examination will focus on their limitations and pitfalls, but also on the opportunities they present for further investigation of moisture damage in building floors using GPR.

4 Discussion

4.1 Laboratory Training Data

As stated above, the observed accuracy gap between training and on-site test data suggests an overfitting of the models to the laboratory data. Examining representative examples from this training data can provide insights into the classifiers decision-making process when applied to new on-site data.

Fig. 11 presents typical measurements for the dry, insulation damage, and screed damage cases from the laboratory experiments. While the B-scans distinctly differ from each other, the A-scan feature distributions reveal notable similarities between the dry measurement and the screed damage measurement. As discussed in the previous laboratory study [26], the uniform screed damages were caused by an evenly distributed moisture ingress across the entire screed sample. Consequently, all features remain relatively constant over the measurement distance. Such a similarity poses a risk of misclassification between a dry floor and screed damage, a concern also observed in the on-site data analysis (Sect. 3.1). For distributions that are similar, the B-scan features also appear alike, as they quantify variations through standard deviation and range. This is demonstrated in Fig. 12, which

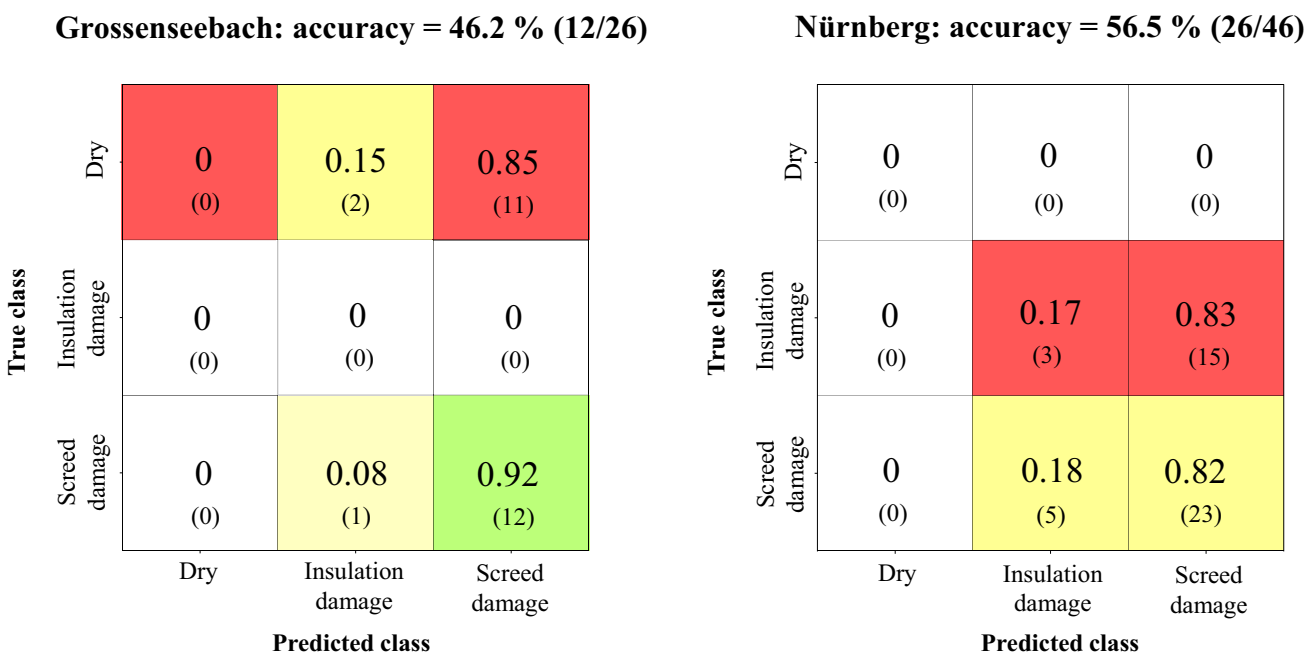

Fig. 10 Classification results of the data sets Grossenseebach and Nürnberg represented by their individual overall accuracy and confusion matrices. Each cell includes the relative (decimal number) and numerical (natural number in brackets) amount of classified cases. The heat map changing from green to red (with yellow as an intermediate color) indicates classification performances, where green represents good accuracy and red represents poor accuracy [27]

presents a scatter plot of the key features F_B and F_D for insulation damage and screed damage cases, respectively. Insulation damage is clearly spaced along the horizontal axis (F_B) in laboratory conditions, whereas data points for laboratory dry cases and screed damage show a similar distribution, with a less distinct separation along the vertical axis (F_D). Consequently, for the laboratory training data, classifiers needed to be finely tuned to slight variations in F_D to effectively distinguish between most of the data points. This concept is further illustrated by the hypothetical decision boundaries depicted in Fig. 12, estimated from the classification accuracy for both laboratory and on-site data. It can be seen that almost all of the more variable on-site data points lie above the defined boundary between screed and insulation damage, indicating that they are likely to be classified as screed damage.

4.2 Variability in On-Site Measurements

This section deals with the question, why the on-site data generally show more variable B-scans than the laboratory experiments. As noted in Sect. 3.1, this could be due to a generally higher heterogeneity in on-site material parameters, such as layer thickness or moisture content, within a single survey line.

This hypothesis is supported by examining the layer thicknesses measured from all cores extracted during the investigations. Figure 13 and 14 summarize these thickness values for the considered and discarded on-site investigations, respectively. Different rooms within the buildings are identified by alternating chart background colors (grey and white). The figures reveal that even within a single room, there can be significant variations in the thicknesses of screed and insulation. Consequently, a 50 cm long survey line is likely to encounter these variations. In real-world scenarios, materials like flow screed [33] or perlites [34] are often used to even out height disparities in floor construction, leading to these thickness variations. Unlike the controlled environment of laboratory experiments where most parameters, including layer thickness, remain constant, on-site measurements can include a wide range of unknown factors. Such variability challenges the basic assumption that deviations in B-scan features are indicative of moisture presence.

Another unknown influence is caused by the spatial limitation of the extracted cores used for reference. This becomes particularly evident when considering the relatively small section a core (6.8 cm diameter) covers compared to an entire survey line (50 cm). The associated difficulties were previously discussed in the context of Fig. 4 b, where a decrease in the amplitude of the direct wave suggested an increase in screed moisture content within the B-scan. To further analyze such indications, examining neighboring MPs is insightful, as demonstrated by MP 40 and MP 34 in Nürnberg (refer to Fig. 15). MP 40, measured along survey line a), show a

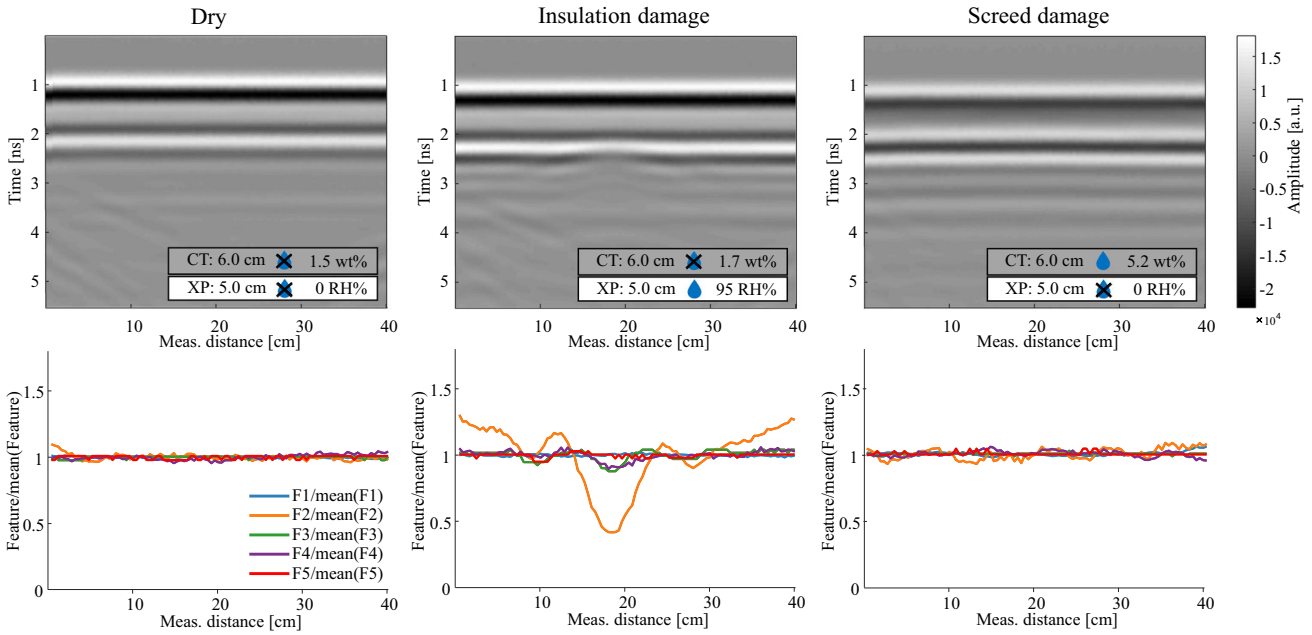

Fig. 11 Exemplary laboratory B-scans (top) and their respective A-scan features (bottom) at an 6 cm CT and 5 cm XP floor construction for the scenarios: dry, damage insulation, and damage screed [27]

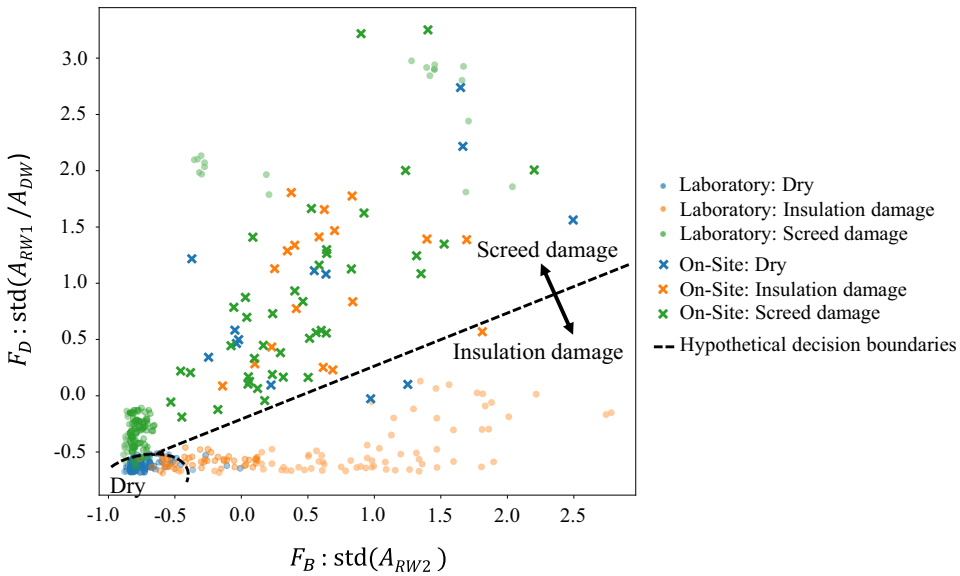

Fig. 12 Scatter plot and hypothetical decision boundaries of B-scan features F_B and F_D for all damage cases within laboratory data and on-site data [27]

referenced moisture damage for both, screed and insulation, while MP 34, measured along survey line b), reveals an insulation damage. The screed moisture content decreased from 4.8 wt% at MP 40 to 3.0 wt% at MP 34. In MP 34 survey line, the antenna moved away from MP 40, revealing a transition from moist to drier screed between 15 cm and 25 cm. The core was positioned off center around 32 cm due to limited access available in the room. It is therefore located in the right half of the B-scan where a decreasing travel time and increasing amplitudes of all wave phases suggest a drier floor setup. This survey line appears to encompass two damage scenarios: screed and insulation damage (similar to MP 40) on the left, and solely insulation damage (as referenced in MP 34) on the right. Figure 16 provides another example, showing neighboring MPs 2 and 3 in Grossenseebach. Here, the screed moisture content declines from 5.1 wt% to 3.0 wt%, while the insulation remains dry for both MPs. The increasing amplitude of the DW and the decreasing travel time of RW1 and RW2 in survey line b) hint at a shift from screed damage to a dry condition.

The ability to discriminate fine details, such as changing moisture states, affirms the resolution and information depth

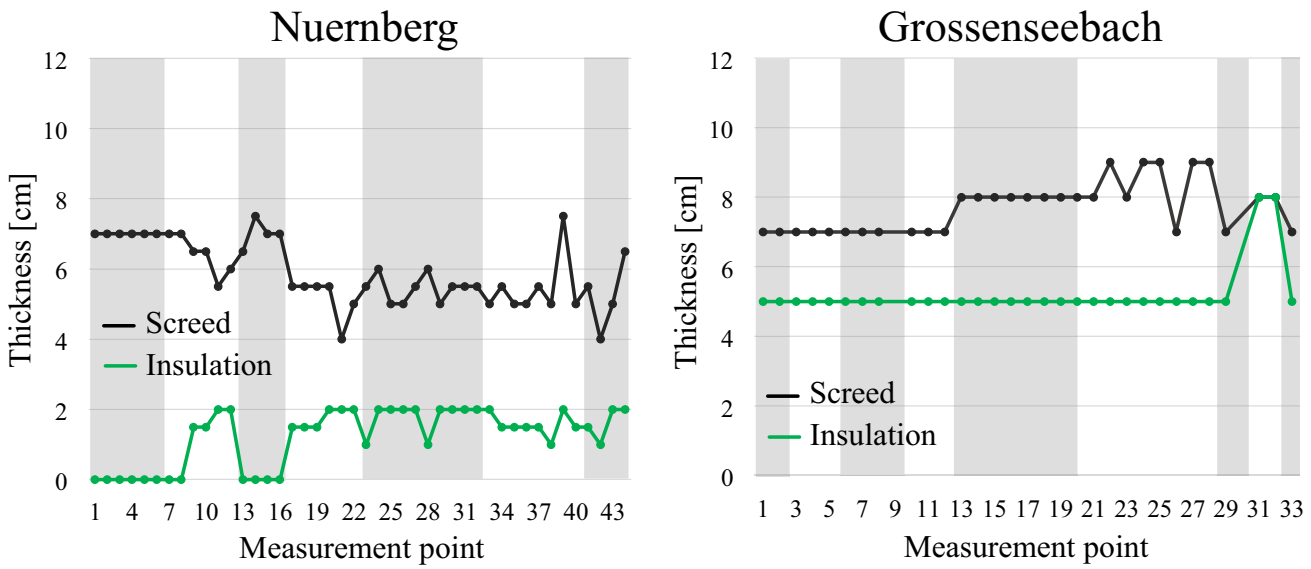

Fig. 13 Layer thicknesses of screed (black) and insulation (green) for every MP in the classified data sets of Nürnberg and Grossenseebach. Chart background colors (grey and white) indicate different rooms [27]

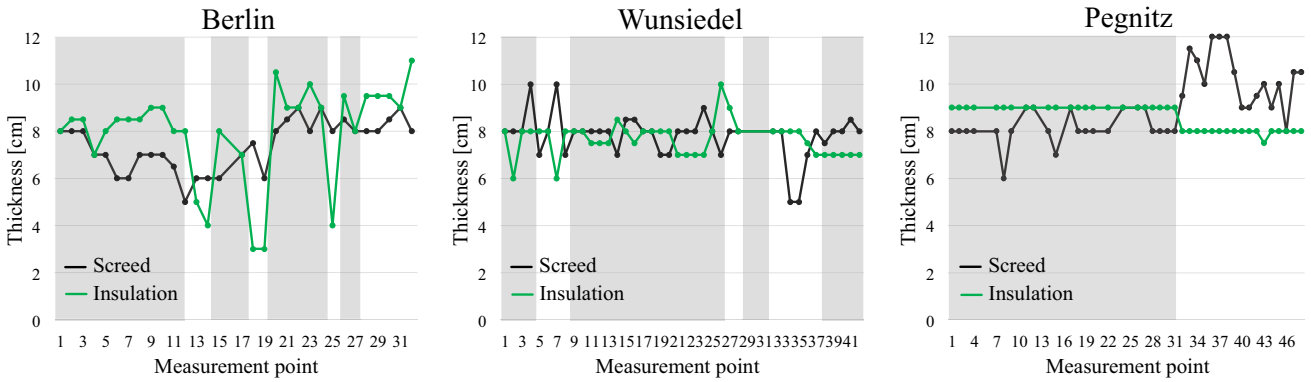

Fig. 14 Layer thicknesses of screed (black) and insulation (green) for every MP in the discarded data sets of Berlin, Wunsiedel, and Pegnitz. Chart background colors (grey and white) indicate different rooms [27]

achievable with GPR in moisture measurements. However, this ability complicates the evaluation of the applied classification strategy. Unlike in laboratory settings, encountering multiple damage scenarios within a single on-site MP is common, which introduces significant uncertainty in classifying an entire B-scan.

4.3 GPR Sensitivity in Damage Detection

Although the application of the automized classification approach achieved lower accuracies, the general sensitivity of GPR and the extracted features for the considered damage cases got clear throughout the investigation. Particularly screed damages, as shown in Figs. 6 and 16 a, provide strong indications by influencing every regarded feature and therefore wave phase. In scenarios where a transition to or from moist screed is visible, like in Figs. 15 b and 16 b, the DW proved to be a valuable source of information, as it is unaffected by changes in the underlying layer thickness. If there is no transition visible, a general danger of confusion to a dry floor setup remains. Here, comparing different MPs may help identifying attenuated DWs, thereby narrowing down areas of potential damage.

In practice, the identification of an insulation damage is even more important, as there are no other sensitive NDT methods available. Also here, the gathered information within the laboratory and the on-site study revealed valuable findings. In addition to the given examples in Figs. 5 and 11, Fig. 17 shows measurements from Nürnberg (MP 17 and MP 24) and from a similar laboratory floor setup. The prominent deviations of RW1 and RW2, captured by F_2, F_3 and F_4, alongside a consistently stable DW, captured by F_1, are strong indicators of higher moisture contents in the insulation layer. In the laboratory, slightly visible reflection hyperbolas were

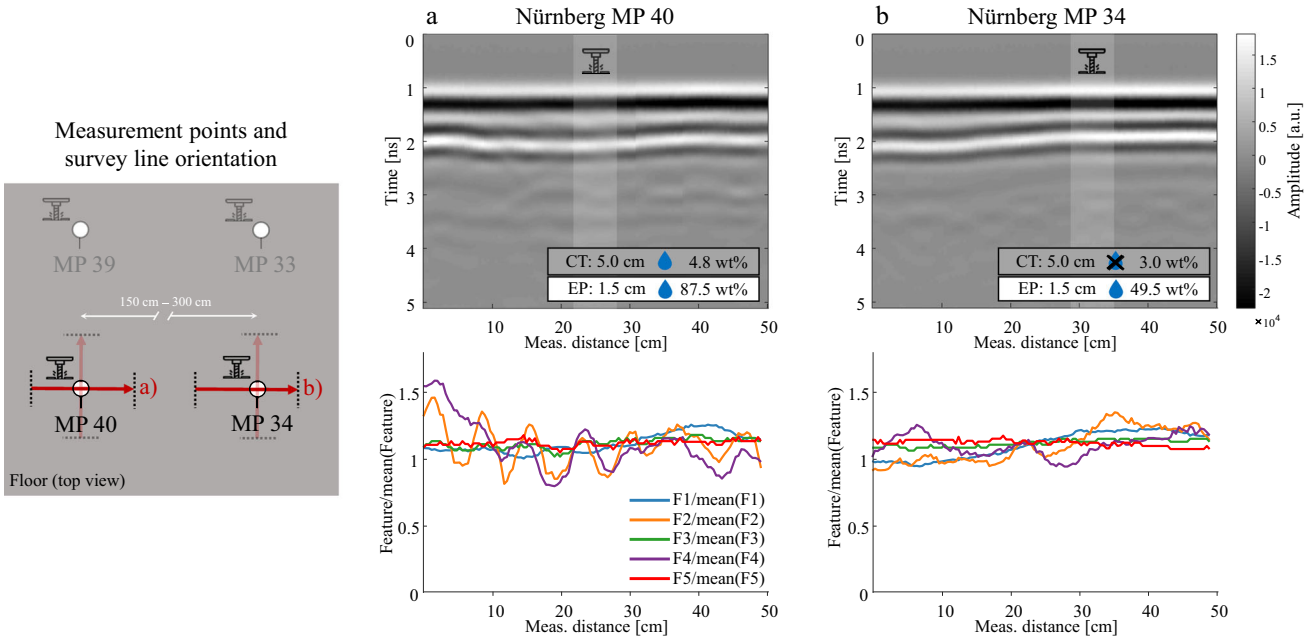

Fig. 15 B-scans and extracted A-scan features of the two neighbouring MPs 40 and 34 in Nürnberg. Survey lines orientation and MPs position are shown on the left [27]

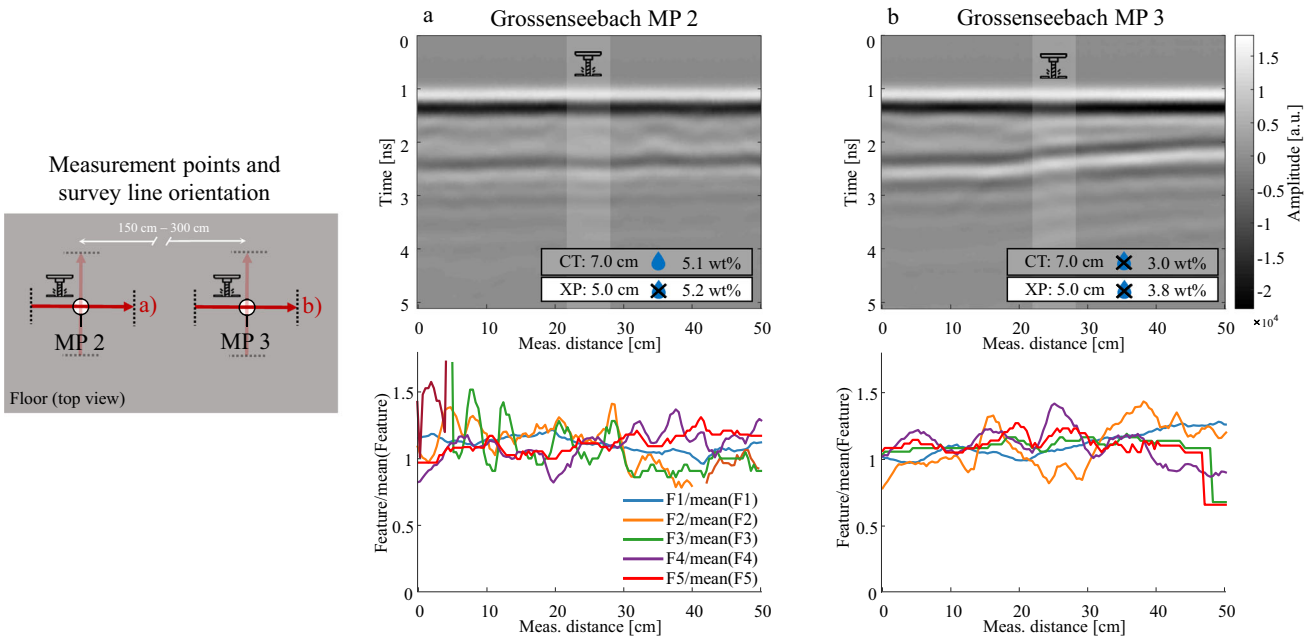

Fig. 16 B-scans and extracted A-scan features of the two neighbouring MPs 2 (**a**) and 3 (**b**) in Grossenseebach. Survey lines orientation and MPs position are shown on the left [27]

noted, resulting from small, highly moist areas, such as fully filled insulation joints - a phenomenon also documented in the laboratory study. The final example demonstrates that, despite the significant differences between on-site and laboratory investigations, useful parallels exist that can aid in analyzing new, practical data. With the increased complexity and unknown variables in on-site scenarios, a solid foundation of knowledge for interpreting results becomes even more crucial. In this context, the considered and extracted features provide substantial support, effectively highlighting variations within a B-scan and assisting in the challenge of accurate interpretation.

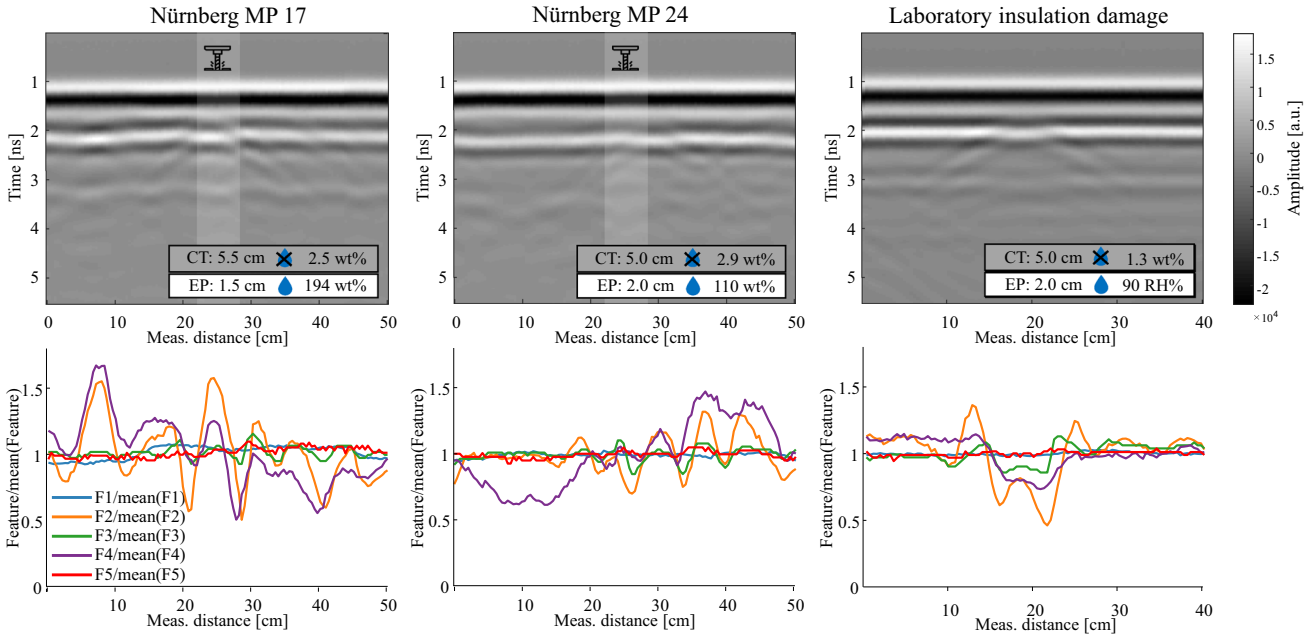

Fig. 17 Exemplary B-scans and A-scan feature distributions of two on-site insulation damages from Nürnberg (MP 17 and MP 24) compared to a similar laboratory floor setup with insulation damage [27]

5 Summary and Conclusion

This study presented the use of classifiers trained by GPR data obtained in a previous laboratory investigation to classify on-site moisture damage scenarios in layered building floors. Five differently affected buildings had been investigated for this purpose. The extraction of cores for each MP served as a reference for material type, layer thickness, and moisture content of both screed and insulation. Thereby, each on-site measurement was labeled with its respective damage scenario, which allowed a quantitative evaluation of the classifier performance.
The main findings of this study are:

- *Lower classification accuracy for on-site damage cases:* Mainly attributable to a significantly higher dynamic of all signal features extracted in on-site measurements compared to laboratory training data.
  Reasons and complicating factors are:
  - Heterogeneous material parameters: changes in screed and insulation layer thicknesses within a survey line hinder clear moisture detection.
  - Varying damage cases: different damage scenarios within a survey line complicate precise classification and highlight the limitations of spatially restricted moisture references.
  - Narrow decision boundary in laboratory data: the close distinction between dry floors and screed damage in laboratory training data often leads to misinterpretation of on-site measurements as screed damage.
- *GPR sensitivity to damage scenarios:*
  - A detailed analysis of individual measurements show the effectiveness of GPR in detecting moisture damage scenarios.
  - Integrating additional information, like results from neighbouring measurement points, proves valuable in eliminating unknown variables and can thereby enhance the reliability of findings.
  - Insulation damages, which often remain unrecognized by other NDT methods, have displayed characteristic patterns within this study.

While the proposed automated classification of moisture damage in layered floors revealed several problems and limitations, individual analysis underlined the opportunities of the GPR method. However, the utilization of this potential still requires trained personnel assessment. The insights gained from this study can serve as a foundation for expanding the expertise of such personnel, enhancing their ability to interpret and analyze GPR data for moisture analysis.

Giving an outlook on future developments, fully automated approaches employing machine learning still would require a substantially larger and more diverse data basis. For the laboratory data, a potential approach to enrich this database could be augmenting it by merging measurements of different setups to simulate varying layer thicknesses of floors. This would provide a more comprehensive range of scenarios. However, it is crucial that realistic on-site data from various scenarios are also included in the training process

to achieve robust and valid decision boundaries. This could either be achieved by an extensive research program or the establishment of an open data repository for GPR and other NDT investigations. The latter is seen as a key element, which would enable machine learning to develop its promising potential within NDT-CE.

In all these efforts, accurate referencing of the data plays a crucial role. Therefore, the extent of moisture-related information must be considerably increased, potentially involving a combination of many procedures. The findings of this work underlined the problem of limited local resolution in extracted cores, where material parameters and damage cases can vary over small distances. Therefore, any limitations in the reference data will directly be reflected in the constraints faced by the trained classifiers, highlighting the need for an accurate and detailed data collection. Only after solving the aforementioned problems in the database, further studies could re-evaluate and optimize the proposed method with respect to the applied signal features and the classification models used.

Other challenges encountered in this work also provide opportunities for future research. A key issue was the presence of underfloor heating, which, based on the recorded measurements, provides insight into the moisture content of the screed. The pronounced reflection hyperbolas observed offer potential for the development of additional features that would allow a more accurate assessment of the radar wave's propagation speed. For this scenario, a laboratory investigation would be beneficial to understand critical parameters such as pipe spacing, their dimensions and materials.

Acknowledgements The authors would like to thank Thomas Kind and Christian Köpp for their helpful comments on the text. For their support in producing the screed samples, gratitude is owed to Hans-Carsten Kühne and Frank Haamkens.

Author Contributions Conceptualization, T.K., C.S., T.R. and S.K.; methodology, T.K., C.S., T.R. and S.K.; software, T.K.; validation, T.K.; formal analysis, T.K.; investigation, T.K.; resources, C.S., T.R. and S.K.; data curation, T.K.; writing-original draft preparation, T.K.; writing-review and editing, T.K., C.S. and S.K.; visualization, T.K.; supervision, C.S. and S.K.; project administration, C.S.; funding acquisition, C.S. and S.K. All authors have read and agreed to the published version of the manuscript.

Funding Open Access funding enabled and organized by Projekt DEAL.

Data Availibility Statement The GPR data underlying this study are openly available in Zenodo at https://doi.org/10.5281/zenodo.10776685 [35]

Declarations

Conflict of interest The authors have no financial or non-financial interests to declare. No external funding was received for conducting this study.

References

1. Harley, J.B., Sparkman, D.: Machine learning and NDE: past, present, and future (2019) https://doi.org/10.1063/1.5099819
2. GDV: Residential Building Insurance: Claims Expenditure by Risk 2003-2022, https://www.gdv.de/gdv/statistik/datenservice-zum-naturgefahrenreport/sachversicherung-naturgefahren/wohngebaeudeversicherung-schadenaufwand-nach-gefahren-2003-2022-139122 (2024). Accessed on 03/06/2024
3. Mendell, M.J., Macher, J.M., Kumagai, K.: Measured moisture in buildings and adverse health effects: a review. Indoor Air **28**(4), 488–499 (2018). https://doi.org/10.1111/ina.12464
4. Annila, P.J., Hellemaa, M., Pakkala, T.A., Lahdensivu, J., Suonketo, J., Pentti, M.: Extent of moisture and mould damage in structures of public buildings. Case Stud. Constr. Mater. **6**, 103–108 (2017). https://doi.org/10.1016/j.cscm.2017.01.003
5. Kruschwitz, S.: Feuchtemessung im Bauwesen - ein Überblick. Fachtagung Bauwerksdiagnose, Vortrag 5 (2014)
6. Nilsson, L.-O.: Methods of Measuring Moisture in Building Materials and Structures. Springer, Berlin (2018). https://doi.org/10.1007/978-3-319-74231-1
7. Chanasky, D.S., Naeth, M.A.: Field measurement of soil moisture using neutron probes. Canadian J. Soul Sci. **76**(3), 317–323 (1996). https://doi.org/10.4141/cjss96-038
8. Huisman, J.A., Hubbard, S.S., Redman, J.D., Annan, A.P.: Measuring soil water content with ground penetrating radar: a review. Vadose Zone J. **2**(4), 476–491 (2003). https://doi.org/10.2113/2.4.476
9. Slater, L., Comas, X.: The Contribution of Ground Penetrating Radar to Water Resource Research. Ground Penetrating Radar: Theory and Applications. Elsevier, London (2009)
10. Lombardi, F., Podd, F., Solla, M.: From its core to the niche: insights from GPR aplications. Remote Sensi. **14**(13), 3033 (2022). https://doi.org/10.3390/rs14133033
11. Lai, W.W.-L., Dérobert, X., Annan, P.: A review of Ground Penetrating Radar application in civil engineering: a 30-year journey from Locating and Testing to Imaging and Diagnosis. NDT&E Int. **96**, 58–78 (2018). https://doi.org/10.1016/j.ndteint.2017.04.002
12. Saarenketo, T., Scullion, T.: Road evaluation with ground penetrating radar. J. Appl. Geophys. **43**(2–4), 119–138 (2000). https://doi.org/10.1016/s0926-9851(99)00052-x
13. Grote, K., Hubbard, S., Harvey, J., Rubin, Y.: Evaluation of infiltration in layered pavements using surface GPR reflection techniques. J. Appl. Geophys. **57**(2), 129–153 (2005). https://doi.org/10.1016/j.jappgeo.2004.10.002
14. Klysz, G., Balayssac, J.-P.: Determination of volumetric water content of concrete using ground-penetrating radar. Cement Concrete Res. **37**(8), 1164–1171 (2007). https://doi.org/10.1016/j.cemconres.2007.04.010

15. Laurens, S., Balayssac, J.P., Rhazi, J., Klysz, G., Arliguie, G.: Non-destructive evaluation of concrete moisture by GPR: experimental study and direct modeling. Mater. Struct. **38**(9), 827–832 (2005). https://doi.org/10.1007/BF02481655
16. Lai, W.L., Kou, S.C., Tsang, W.F., Poon, C.S.: Characterization of concrete properties from dielectric properties using ground penetrating radar. Cement Concrete Res. **39**(8), 687–695 (2009). https://doi.org/10.1016/j.cemconres.2009.05.004
17. Garrido, I., Solla, M., Lagüela, S., Fernández, N.: IRT and GPR techniques for moisture detection and characterisation in buildings. Sensors **20**(22), 6421 (2020). https://doi.org/10.3390/s20226421
18. Lai, W.L., Kind, T., Kruschwitz, S., Wöstmann, J., Wiggenhauser, H.: Spectral absorption of spatial and temporal ground penetrating radar signals by water in construction materials. NDT & E Int. **67**, 55–63 (2014). https://doi.org/10.1016/j.ndteint.2014.06.009
19. Hola, A.: Measuring of the moisture content in brick walls of historical buildings - the overview of methods. IOP Conf. Series: Mater. Sci. Eng. **251**, 012067 (2017). https://doi.org/10.1088/1757-899X/251/1/012067
20. Kurz, F., Sgarz, H.: Measurement of Moisture Content in Building Materials using Radar Technology. International Symposium Non-Destructive Testing in Civil Engineering (NDT-CE) (2015)
21. Davis, J.L., Annan, A.P.: Electromagnetic detection of soil moisture: progress report I. Canadian J. Remote Sens. **3**(1), 76–86 (1977). https://doi.org/10.1080/07038992.1977.10854959
22. Soutsos, M.N., Bungey, J.H., Millard, S.G., Shaw, M.R., Patterson, A.: Dielectric properties of concrete and their influence on radar testing. NDT&E Int. **34**(6), 419–425 (2001). https://doi.org/10.1016/S0963-8695(01)00009-3
23. Daniels, D.J.: Ground Penetrating Radar. The Institution of Engineering and Technology., 2nd edn. Elsevier, London (2004)
24. Topp, G.C., Davis, J.L., Annan, A.P.: Electromagnetic determination of soil water content: measurements in coaxial transmission lines. Water Resour. Res. **16**(3), 574–582 (1980). https://doi.org/10.1029/WR016i003p00574
25. Klewe, T., Strangfeld, C., Kruschwitz, S.: Review of moisture measurements in civil engineering with ground penetrating radar - applied methods and signal features. Constr. Build. Mater. **278**, 122250 (2021). https://doi.org/10.1016/j.conbuildmat.2021.122250
26. Klewe, T., Strangfeld, C., Ritzer, T., Kruschwitz, S.: Combining signal features of ground-penetrating radar to classify moisture damage in layered building floors. Appl. Sci. **11**(19), 8820 (2021). https://doi.org/10.3390/app11198820
27. Klewe, T.: Non-destructive classification of moisture deterioration in layered building floors using ground penetrating radar. Doctoral Thesis (2023) https://doi.org/10.14279/depositonce-19306
28. ASTM D2216-19: Standard Test Methods for Laboratory Determination of Water (Moisture) Content of Soil and Rock by Mass. ASTM Vol. 04.08 (2019)
29. Klewe, T., Strangfeld, C., Ritzer, T., Kruschwitz, S.: Nondestructive determination of moisture damage in layered building floors. SEG Global Meeting Abstracts, 18th International Conference on Ground Penetrating Radar (2020) https://doi.org/10.1190/gpr2020-045.1
30. Pedregosa, F., Varoquaux, G., Gramfort, A., Michel, V., Thirion, B., Grisel, O., Blondel, M., Prettenhofer, P., Weiss, R., Dubourg, V., Vanderplas, J., Passos, A., Cournapeau, D., Brucher, M., Perrot, M., Duchesnay, E.: Scikit-learn: machine learning in python. J. Machine Learn. Res. **12**, 2825–2830 (2011). https://doi.org/10.5555/1953048.2078195
31. Breiman, L.: Bagging predictors. Machine Learn. **24**(2), 123–140 (1996). https://doi.org/10.1007/BF00058655
32. Dietterich, T.: Overfitting and undercomputing in machine learning. ACM Comput. Surv. **27**(3), 326–327 (1995). https://doi.org/10.1145/212094.212114
33. Canbaz, M., Topçu, İB.: Ateşin: efect of admixture ratio and aggregate type on self-leveling screed properties. Constr. Build. Mater. **116**, 321–325 (2016). https://doi.org/10.1016/j.conbuildmat.2016.04.084
34. Singh, M., Garg, M.: Perlite-based building materials — a review of current applications. Constr. Build. Mater. **5**(2), 75–81 (1991). https://doi.org/10.1016/0950-0618(91)90004-5
35. Klewe, T., Strangfeld, C., Ritzer, T., Kruschwitz, S.: GPR dataset of moisture measurements on building floors in laboratory and on-site. Zenodo (2024). https://doi.org/10.5281/ZENODO.10776685